J-Researchers

JOURNAL OF CIVIL ENGINEERING RESEARCHERS

Investigating and comparing the performance of common composite columns

[a]Sadeghian S.*

[a]"Junior, Faculty of Engineering, Chalous Branch, Islamic Azad University, Chalous, Iran"

Journals-Researchers use only: Received date here; revised date here; accepted date here

Abstract

In this article, I have tried to collect a set of functions of different types of composite columns. For the first time, a set of articles and the performance of different types of composite columns are studied, reviewed and compared. Some of the influential factors are: study of the behavior of various buckling modes, their performance under compressive loading with and without eccentricity, study of local and general buckling of composite columns, factors causing confinement in composite columns, behavior of these columns in different strength ranges from concrete alone Normal strength to high strength concretes, also the performance of these columns under the influence of steels with different yield stresses, the effect of behavioral performance of changing the thickness of steel hollow pipes, the presence or absence of steel profiles in the core of composite columns and finally to verify the results The laboratory is compared with numerical methods by software to confirm the accuracy of laboratory work as much as possible

"Keywords: composite columns ; steel reinforced concrete ; concrete ; steel ; concrete filled tube"

1. Types of composite columns and introduction of the studied models

Composite columns are columns that have both the advantages of steel and concrete. Composite columns are made with different sections, hence they have structural diversity. Composite columns are divided into the following general groups according to the location of concrete and steel, which are:

a. concrete filled tube: These columns include hollow, rectangular, or polygonal hollow steel sections, which are filled with concrete.

b. steel reinforced concrete: In this group, the steel section is surrounded by reinforced concrete. In other words, this section includes a rolled or composite steel section that is buried inside a section of reinforced concrete.

1.1 An introduction *to concrete encased steel composite columns*

* e-mail: samet.sadeghian@iauc.ac.ir

Composite columns are frequently used in high-rise buildings. Some of the virtues of utilizing these columns are high strength, full use of materials, high hardness, high ductility, resistance against seismic loads, and the fact that they can be constructed in a shorter amount of time. Composite columns are produced of steel core encased by concrete (SRC) or hollow steel tube filled with concrete (CFT). One of the superiorities of SRC columns to CFT columns is their high fire resistance.

Experimental investigations on concrete encased steel composite columns have been conducted by Anslijn and Janss [1], Matsui [2], Mirza and Skrabek [3], Mirza et al. [4], Chen and Yeh [5], Tsai et al. [6], Chen et al. [7], El-Tawil and Deierlein [8] and Dundar et al. [9] Shanmugam and Lakshmi [10]. These tests were carried out on concrete encased steel composite columns having different slenderness ratios, different steel sections and different concrete and steel strengths. On the other hand, analytical studies on concrete encased steel composite columns have been performed by Furlong [11], Virdi and Dowling [12], Roik and Bergmann [13], Kato [14] and Chen and Lin [15]. However, to date no detailed nonlinear 3-D finite element model was found in the literature highlighting the behavior of concrete encased steel composite columns. This is attributed to the complexity of the concrete confinement, steel–concrete interface, longitudinal reinforcement bar–transverse reinforcement bar interface, and reinforcement bar–concrete interface as well as the nonlinear constitutive stress–strain curves of the composite column components.

1.2. Concrete filled steel tube columns (CFST and SRCFST)

In the past few decades, CFST columns have been extensively used in the construction of bridges and modern buildings [16]. The origin of these columns dates back to 1879 when they were first employed in the pillars of railway bridges in Severn, England [17]. They have also proved to be practical in areas with a greater risk of earthquakes. These structures are advantageous when they encompass a combination of steel and concrete tubes. Such structures can be built at a higher speed and in addition to that, they will have less weight with higher bending stiffness. They also have performed more successfully in the presence of cyclic loading compared to reinforced concrete structures.

SRCFSTs are a new type of composite columns [16] which comprise I-shaped steel sections, reinforced concrete, and hollow steel tubes filled with concrete [18]. An illustration of these sections has been presented in Figure (1). These sections function as an integrated group. As SRCFST columns incorporate the advantages of both types of columns SRC and CFST, this combination leads to a better performance in buildings.

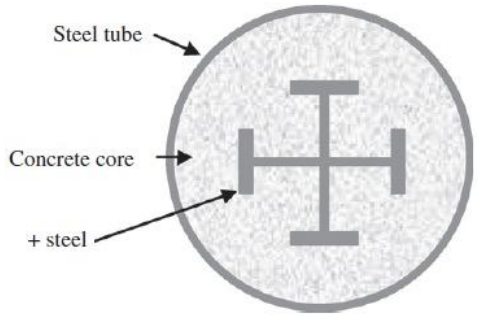

figure 1. SRCFST column cross section[19]

1.3. Square self-compacting concrete columns (SCC)

One of the main positive aspects of these columns is their high load-bearing capacity, inherent flexibility and high level of hardness [20, 21]. Self-compacting concrete has been received well by civil engineers in recent years [22, 23]. Another benefits of this type of concrete is that it compacts under its weight and therefore no vibrator or other vibrating device will be necessary, which results in the prevention of noise pollution in the environment and less need for the workforce.

1.4. Elliptical hollow sections filled with concrete

Elliptical hollow columns (EHS) are more appealing than circular and square columns and also have a greater resistance to loading. Although the behavior of elliptical columns can be predicted from the behavior of circular and square columns, their behavior needs to be separately investigated

nevertheless. The behavior of hollow elliptical columns has been tested under cross-sectional compressive strength, bending strength, and shear strength. Previous research into the behaviour and design of unfilled EHS has included investigations of cross-section compression resistance[24], bending resistance [25] and shear resistance [26]. Slenderness limits to account for local buckling under various loading configurations have also been developed [24, 25, 27].

2. A review of other models and studies

2.1. SRC composite columns with no eccentricity

E.Ellobody and B.Young [28] conducted an examination of some parts of the concrete-encased composite columns such as longitudinally reinforcing bars, transverse reinforcing bars, steel profiles, and finally backfill concrete illustrated in Figure (2). Earlier researches by Sheikh et al. [29] and Mander et al. [30] on reinforced concrete columns have shown that confinement provided by the reinforcement bars creates two zones in the concrete column.

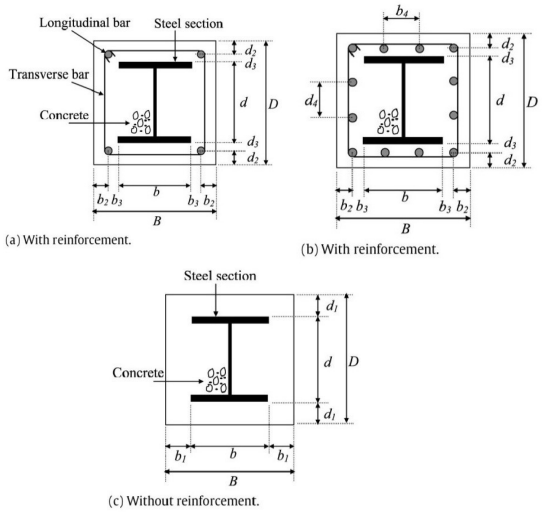

Figure 2. Concrete encased steel composite[28]

The components of the concrete-encased steel composite column have been simulated using a combination of 3-D solid (C3D8 and C3D6) elements in the ABAQUS finite element software [31]. The elements have 3 degrees of freedom in each node; and these conditions extend to all column components. For uniaxial loading, in both cases of confinement and unconfinement, f_c=0.8f_{cu} and ε_c=0,003 have been defined based on ACI [32]. The equations between unconfined and confined concrete for compressive strength and strain are developed by Mander et al. Confinement factor for concretes with full confinement between -1 and 1 is 1.97. These values depend on various factors such as the distance between the bars, the shape of the building profile. On the other hand, the confinement factor for concrete with incomplete confinement between -1 and 0.9 is considered to be 1.5; and the confinement factor is also dependent on the shape of the steel profile and the intervals between the transverse bars. K2=20.5 , K1 =0.1 [33] Also, the refractive energy (G_f) in this paper is suggested to be 0.12 [34]. The buckling mode of steel composite columns surrounded by concrete is created. The actual geometry and properties of the materials are attained by conducting the special buckling analysis. The lowest buckling mode is the buckling mode (No. 1) which is used in the analysis of properties. SRC columns under eccentric loading are simulated using C3D8 and C3D6 elements in Abacus software [32].

2.2. SRC composite columns with eccentricity:

SRC columns under eccentric loading are introduced to Abaqus software using C3D8 and C3D6 elements [31]. Parameters related to concrete confinement including $(\varepsilon_{cc}, f_{cc}, U_{cc}, \ldots$ are stated in the same way as SRC columns, which have already been mentioned. It should be noted that Ecc is calculated using the following equation [32, 34].

$$E_{cc} = w_c^{1.5} 0.043 \sqrt{f_{cc}} Mpa$$

The properties of steel materials in the linear part of the stress-strain curve, as well as nonlinear part, are the same as in the SRC specimen without the eccentricity of the load.

Table 1. Geometric and material properties of all samples tested[35]

Specimen ID	Steel tube		Section steel			Concrete compressive strength f_{cu} (MPa)	n
	$D \times t$ (mm)	Yield strength, f_{y1} (MPa)	I steel	A_s (mm^2)	Yield strength, f_{y2} (MPa)		
HC12-1	218 × 4	269	I12	3570	314	74.3	0.50
HC12-2	218 × 4	269	I12	3570	314	74.3	0.66
HC14-1	218 × 4	269	I14	4160	305	74.3	0.50
HC14-2	218 × 4	269	I14	4160	305	74.3	0.66
HC14-3	218 × 4	269	I14	4160	305	74.3	0.50

Table 2. Specifications and results of samples[36]

Specimen	$B \times t \times L_0$ (mm)	L/B	f_c (MPa)	A_c (mm^2)	f_{yt} (MPa)	A_t (mm^2)	f_{ys} (MPa)	A_s (mm^2)	ρ_{ss}	μ_{85}	N_u^{exp} (kN)	N_u^{nom} (kN)	$\frac{N_u^{exp}}{N_u^{nom}}$
S5L10V	195 × 5.5 × 600	3	48.4	30990	288	4169	338	2866	0.085	a*	4035	3669	1.10
S5L10	195 × 5.5 × 600	3	48.4	30990	288	4169	338	2866	0.085	a	4050	3669	1.10
S5H10V	195 × 5.5 × 600	3	70.8	30990	288	4169	338	2866	0.085	2.77	4880	4363	1.12
S5H10	195 × 5.5 × 600	3	70.8	30990	288	4169	338	2866	0.085	2.34	4880	4363	1.12
S4L10	195 × 4.5 × 600	3	48.4	31730	289	3429	338	2866	0.083	a	3930	3495	1.12
S4H10	195 × 4.5 × 600	3	70.8	31730	289	3429	338	2866	0.083	2.16	4750	4206	1.13
S4L10I	195 × 4.5 × 600	3	48.4	33163	289	3429	338	1433	0.041	2.04	3410	3080	1.11
S4H14	195 × 4.5 × 600	3	70.8	30726	289	3429	327	4300	0.123	2.90	4710	4572	1.03
S5L10I	195 × 5.5 × 600	3	48.4	32423	288	4169	338	1433	0.042	2.75	3620	3254	1.11
S5L10C	195 × 5.5 × 600	3	48.4	30990	288	4169	338	2866	0.085	a	3860	3669	1.05
S5H10C	195 × 5.5 × 600	3	70.8	30990	288	4169	338	2866	0.085	2.58	4980	4363	1.14
S4L	195 × 4.5 × 600	3	48.4	34596	289	3429	–	0	0.000	1.81	2985	2665	1.12
S4H	195 × 4.5 × 600	3	70.8	34596	289	3429	–	0	0.000	1.78	3900	3440	1.13
L4L10-6	195 × 4.5 × 1200	6	48.4	31730	289	3429	338	2866	0.083	–	3765	3495	1.08
L4L10-9	195 × 4.5 × 1800	9	48.4	31730	289	3429	338	2866	0.083	–	3720	3495	1.06
L4L10-12	195 × 4.5 × 2400	12	48.4	31730	289	3429	338	2866	0.083	–	3410	3495	0.98
L5L10I-9	195 × 5.5 × 1800	9	48.4	32423	288	4169	338	1433	0.042	–	3520	3254	1.08
L5L10I-12	195 × 5.5 × 2400	12	48.4	32423	288	4169	338	1433	0.042	–	3245	3254	1.00

* a—the axial load did not fall to 85% of the maximum load when the test stopped.

2.3. Composite Columns SRCCFT:

Chang et al. [19] investigated the behavior of steel under cyclic loading in a linear kinematic hardening model. For modeling sections after the yield-point the hardness of steel is considered to be 1% of Yang modulus for steel materials.

Both shell and solid elements can be used to introduce the components of a hollow steel tube [22, 37, 38] owing to the symmetrical shape of the column, only half of the composite column is modeled. The interaction used between hollow steel tube and concrete is of the surface type.

5 specimens are used for numerical validation of the models [38] which have been compared with the experimental method. These 5 specimens can be divided into two groups of HC12, HC14, which have two various types of steel profiles. In both sample groups, the level of axial force (n) is between 0.5 and 0.66. The geometric characteristics and parameters are comprehensively listed in Table (1).

2.4. Composite columns with self-compacting concrete

Zhu et al. [36] carried out some experiments on square hollow metal columns filled with high-strength concrete. The experimental parameters and dimension of the specimens have been exhaustively demonstrated in Figure (3) and Table (2):

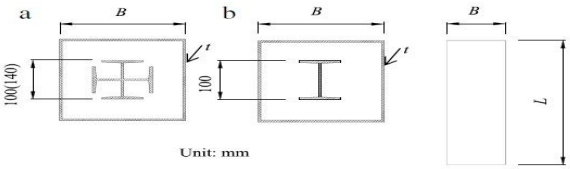

Figure 3. Test specimens: (a) Cross section of cross section steel profile (b) Cross section of steel profile with I cross section[36]

In the labels given to the specimens, the first letter denotes the type of specimen (S denotes the short specimens and L represents the long ones). The first number indicates the tube thickness in millimetres,

the second letter indicates the strength of concrete (L indicates f_c=48.4, and accordingly H Indicates concrete with strength of f_c=7 0.8). The second number indicates the height of the steel cross-section in centimetres (removing this number indicates that the steel section is not confined). The third letter denotes the special design variables. (V denotes vibrated concrete and I denotes the shape of steel profile, and C represents cyclic loading. The removal of these letters indicates that the concrete is self-compacting, and also means that the concrete is under uniform loading.).

All specimens have been tested using an impact testing machine with a bearing capacity of 5000 KN [36]. The design and procedure of performing the tests by the machine have been shown in Figure (4). A set of 4 strain gauges have been attached to the flanges of steel section in the middle part of the section height which measure the axial and lateral strains of the member and 12 strain gauges have been attached to the lateral surface of the steel frame to measure the axial deformation and the expansion of wall surrounding.

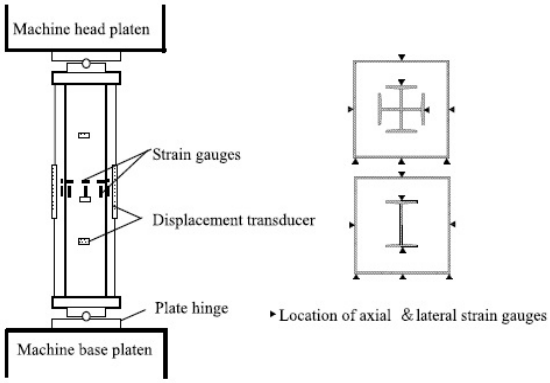

Figure 4. How to perform the test on the sample[36]

2.5. Experimental studies on the cross-section of hollow elliptical tubes filled with concrete

Some studies were conducted on this type of column by Yang et al. [17]. To do so, a selection of 21 elliptical hollow sections filled with concrete was tested [17]. Some experimental tensile and attrition tests have been carried out on the same types of materials with properties similar to the one mentioned above by Imperial University of London [24]. 9 specimens out of a total of 21 had been under composite loading without greasing between concrete and steel tube. 6 of these specimens were tested under composite loading, but this time, the inner surface of the steel tube had been coated with a layer of grease before performing the shrinkage test; and finally, the last 6 specimens were core-loaded (none-greased). 3 types of steel tubes with 3 nominal thicknesses of 4, 5, and 6.3 mm and 3 concrete grades of c100, c60, and c30 were used. Specimens with 4 and 5 mm in thickness were classified as slender and the 6.3 specimens considered to be fully effective.

All 21 concrete-filled elliptical specimens were tested under compression in a 3000 kN capacity ToniPACT 3000 testing machine. Three horizontal strain gauges (to measure hoop strains) and one vertical strain gauge (to measure axial strains) were affixed to each specimen, as shown in Fig, 5. All strain gauges were positoonedon the outer circumference of the elliptical steel tubes. Axial shortening of the specimens was captured by means of a linearvariable displacement transducer (LVDT) positioned between the end platens of the testing machine. For the core-loaded specimens, blocks were utilized at the two ends of the specimens to achieve uniformly transferred loading.

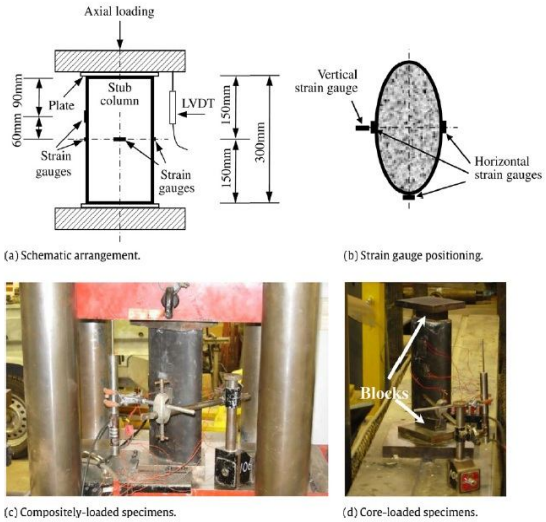

Figure 5. Installation of samples for testing [17]

Table 3. Dimensions and material properties of SRC columns[28]

Test	Dimensions			Steel section	Reinf.	Material properties			Ref.
	B (mm)	D (mm)	kL_e (mm)			Concrete strength (MPa)	f_{ys} (MPa)	f_{yr} (MPa)	
17	240	240	1282	H 140 × 140 × 7 × 12	–	29.2[a]	276	376	
15	240	240	2488	H 140 × 140 × 7 × 12	–	33.6[a]	276	376	[1,15]
12	240	240	3478	H 140 × 140 × 7 × 12	–	35.1[a]	293	376	
21	240	240	3485	H 140 × 140 × 7 × 12	–	32.0[a]	380	376	
1	160	160	924	H 100 × 100 × 6 × 8	Fig. 1(a)	18.5[a]	306	376	
2	160	160	2309	H 100 × 100 × 6 × 8	Fig. 1(a)	21.4[a]	298	376	[2,15]
3	160	160	3464	H 100 × 100 × 6 × 8	Fig. 1(a)	22.5[a]	304	376	
A	165.1	177.8	229	UB 127 × 114 × 29.76	Fig. 1(a)	18[b]	248	376	
B	165.1	177.8	1168	UB 127 × 114 × 29.76	Fig. 1(a)	18[b]	248	376	[3]
C	165.1	177.8	2083	UB 127 × 114 × 29.76	Fig. 1(a)	18[b]	248	376	
SRC1	280	280	1200	H 150 × 150 × 7 × 10	Fig. 1(b)	29.5[b]	296	350	
SRC2	280	280	1200	H 150 × 150 × 7 × 10	Fig. 1(b)	28.1[b]	296	350	[6,7]
SRC3	280	280	1200	H 150 × 150 × 7 × 10	Fig. 1(b)	29.8[b]	296	350	

[a] Denotes concrete cube strength.
[b] Denotes concrete cylinder strength.

Table 4. Details of composite sections and details of its reinforcing bars[28]

Test	Composite section dimensions (mm)										Reinforcement				Ref.
	b	b_1	b_2	b_3	b_4	d	d_1	d_2	d_3	d_4	Long.		Transverse		
											No	Ø	S	Ø	
17	140	50	–	–	–	140	50	–	–	–	–	–	–	–	
15	140	50	–	–	–	140	50	–	–	–	–	–	–	–	[1,15]
12	140	50	–	–	–	140	50	–	–	–	–	–	–	–	
21	140	50	–	–	–	140	50	–	–	–	–	–	–	–	
1	100	30	19	11	–	100	30	19	11	–	4	6	75	4	
2	100	30	19	11	–	100	30	19	11	–	4	6	75	4	[2,15]
3	100	30	19	11	–	100	30	19	11	–	4	6	75	4	
A	114.3	25.4	14.4	11	–	127	25.4	14.4	11	–	4	6	75	4	
B	114.3	25.4	14.4	11	–	127	25.4	14.4	11	–	4	6	75	4	[3]
C	114.3	25.4	14.4	11	–	127	25.4	14.4	11	–	4	6	75	4	
SRC1	150	65	34	31	88	150	65	34	31	88	12	12	140	8	
SRC2	150	65	34	31	88	150	65	34	31	88	12	12	75	8	[6,7]
SRC3	150	65	34	31	88	150	65	34	31	88	12	12	35	8	

Table 5. Compare experimental results and finite element results[28]

Test [Ref.]	$\bar{\lambda}$	Test		EC4	AISC	FE			P_{FE}/P_{Test}	P_{Test}/P_{EC4}	P_{Test}/P_{AISC}
		P_{Test} (kN)	Failure mode	P_{EC4}	P_{AISC}	P_{FE} (kN)	e_{FE} (mm)	Failure mode			
17 [1,15]	0.25	2471	CC + SY	2163	2083	2367	3.40	CC + SY	0.96	1.14	1.19
15 [1,15]	0.48	2344	CC + SY	2019	1887	2271	6.34	CC + SY	0.97	1.16	1.24
12 [1,15]	0.70	2579	F	1815	1544	2539	11.4	F	0.98	1.42	1.67
21 [1,15]	0.74	2471	F	1919	1619	2495	6.56	F	1.01	1.29	1.53
1 [2,15]	0.26	996	CC + SY	951	921	1009	2.07	CC + SY	1.01	1.05	1.08
2 [2,15]	0.66	974	F	759	682	868	3.28	F	0.89	1.28	1.43
3 [2,15]	1.29	874	F	567	423	800	4.24	F	0.92	1.54	2.07
A [3]	0.06	1566	CC + SY	1360	1356	1708	5.07	CC + SY	1.09	1.15	1.15
B [3]	0.33	1370	CC + SY	1270	1248	1396	2.76	CC + SY	1.02	1.08	1.10
C [3]	0.59	1366	CC + SY	1076	1036	1231	2.72	CC + SY	0.90	1.27	1.32
SRC1 [6,7]	0.19	4220	CC + SY	3809	3655	4145	4.87	CC + SY	0.98	1.11	1.15
SRC2 [6,7]	0.19	4228	CC + SY	3723	3574	4033	4.67	CC + SY	0.95	1.14	1.18
SRC3 [6,7]	0.19	4399	CC + SY	3828	3672	4214	3.95	CC + SY	0.96	1.15	1.20
Mean	–	–	–	–	–	–	–	–	0.97	1.21	1.33
COV	–	–	–	–	–	–	–	–	0.055	0.117	0.211

Note: CC denotes Concrete Crushing, SY denotes Steel Yielding and F denotes Flexural buckling.

3. Parametric analysis and studies on the specimens

3.1 SRC composite steel columns without the eccentricity of the loading

Tables (3) and (4) provide the details of the dimensions and size of the specimens as well as the properties of the materials.It should be noted that 3 buckling modes as well as main variables in the tests on SRC columns have been provided in Table (5) .

Various types of failure modes occurred in the specimens of these tests are as follows:
(CC): Failure mode for crushing of the concrete (concrete crushing)
(SY): Failure due to the yielding of the steel (steel yielding)
(F): Flexural buckling mode

These three modes can be simply examined and tested by measuring the stresses in the concrete and structural steel elements and their capability to withstand these stresses. The first two modes occur concurrently. The yielding occurs in the flange of the steel section with the appearance of the first crack in the concrete in the columns with $\bar{\lambda} \leq 0.59$. On the other hand, the flexural buckling mode was observed when $0.66 \leq \bar{\lambda} \leq 1.29$. It should be noted that in concrete failure mode, concrete failure under compression and yielding of structural steel are simultaneous whereas the failure of the concrete due to tensile fracture takes place before the steel reaches the yield stress.

A total of 48 samples of composite columns have been analyzed in parametric studies. The structural steel yielding and concrete crushing (CC+SY) are observed to occur concurrently when $\bar{\lambda} \leq 0.59$ and flexural buckling failure mode takes place when $\bar{\lambda} > 0.59$. The effect of structural steel yield stress and concrete strength on the strength of composite columns encased by reinforced concrete for groups G4-G12 has been indicated in Figure (6).

It should be pointed out that an increase in the strength of structural steel results in only an insignificant effect on the strength of composite columns. An increase in the strength of steel has no considerable effect on the strength of the column in the case of reinforced composite columns with $\bar{\lambda} \geq 0.89$ whereas the utilization of steel with high levels of strength results in a substantial elevation in the strength of composite columns in short columns.

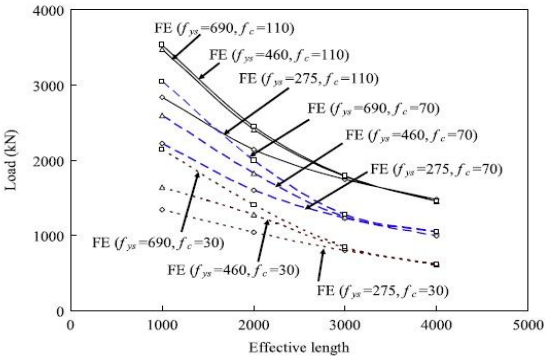

Figure 6. Effect of structural steel yield stress and concrete strength on the strength of G4-G12 composite columns[28]

3.2. SRC composite steel columns with the eccentricity of the loading

The eccentricity of the load attained from the tests have been compared with the data obtained from finite elements, and a summary of this comparison has been indicated in Table (6). This obviously a demonstration of a great consistency between the results obtained from the finite elements and experimental results.

Table 6. Comparison between finite element and experimental results[39]

Test [Ref.]	Test	FE		P_{FE}/P_{Test}
	P_{Test} (kN)	P_{FE} (kN)	Failure mode	
BC1 [11]	654	601	F	0.92
BC2 [11]	558	511	F	0.92
BC3 [11]	962	827	F	0.86
BC4 [11]	949	946	F	1.00
BC5 [11]	900	822	F	0.91
BC6 [11]	813	684	F	0.84
BC7 [11]	704	583	F	0.83
BC8 [3]	1014	1043	F	1.03
BC9 [3]	996	977	F	0.98
BC10 [3]	747	740	F	0.99
BC11 [3]	716	742	F	1.04
BC12 [3]	529	522	F	0.99
BC13 [4]	740	660	F	0.89
BC14 [4]	504	530	F	1.05
BC15 [4]	412	406	F	0.99
Mean	–	–	–	0.95
COV	–	–	–	0.077

A total of 54 specimens of SRC columns with various levels of the eccentricity of the load, cross-sectional dimensions, structural steel type, concrete strength, and the yield stress of structural steel. It is worth noting that that only the buckling mode in these specimens is the mode of flexural buckling.The strengths of different eccentric-loaded SRC columns in the specimens of (G1-G9) with a square cross-section against different amounts of concrete strength have been illustrated in Figure (7). It is can be observed that the curves for columns with $e \leq 0.125D$ are almost linear. Any increase in the concrete strength and the yield stress of structural steel results in an increase in the strength of composite columns.

Considering an overall summary of the results, it can be concluded that there is a significantly positive relationship between the effect of the strength of SRC columns and yield stress of structural steel, that is, for columns with e <0.125 D and with concrete strength lower than 70 MPa, the effect of the strength of SRC columns significantly increases with the increase of yield stress of structural steel.

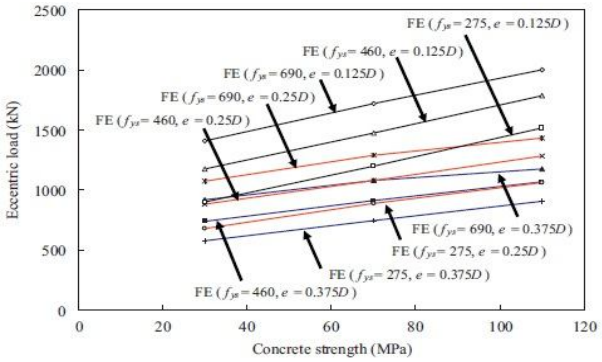

Figure 7. Effect of concrete strength on the strength of SRC square columns with eccentricity for G1-G8 groups[39]

Column strength and concrete strength are also related for specimens (G10-G18) with a rectangular cross-section as shown in Fig (8). Contrary to (G1-G9) composite columns the linear relation are observed for all composite columns and an increase in the strength of the columns is linked with the increase of yield stress in structural steel

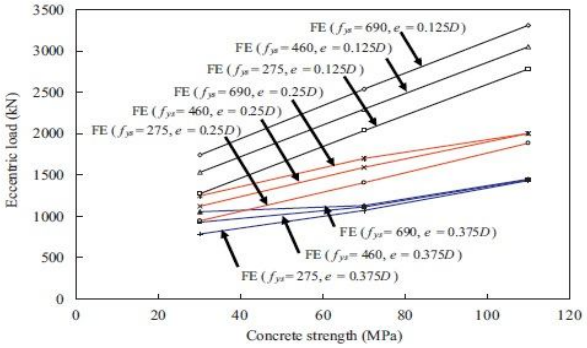

Figure 8. The effect of concrete strength on the strength of SRC rectangular columns with eccentricity for G10-G18 groups[39]

3.3. SRCFST composite columns

Figure (9) indicates the longitudinal stress distribution in the cross-sectional of the concrete core in both types of CFST and SRCFST columns. At the time that the hollow square steel section reaches the yield strength point, although the tensile section in SRCFST columns is, in fact, less than CFST columns, the figures suggest that generally, the tensile section in SRCFST columns is similar to that in CFST columns until graph reaches point 3. The reason for this is the presence of steel section which can prevent the expansion of fracture in the tensile area when it is loaded with external forces.

It can also be observed that the maximum amount of longitudinal stress will take place at the section of the concrete core in the center of the SRCFST columns. The maximum longitudinal stress for CFST columns, however, occurs in the section of the concrete core near the flanges as indicated in Fig (9). This allows for the flanges to provide confinement in the internal concrete. It can be generally concluded that SRCFST columns have evidently more levels of hardness and greater yield strength compared to CFST columns Figure (10).

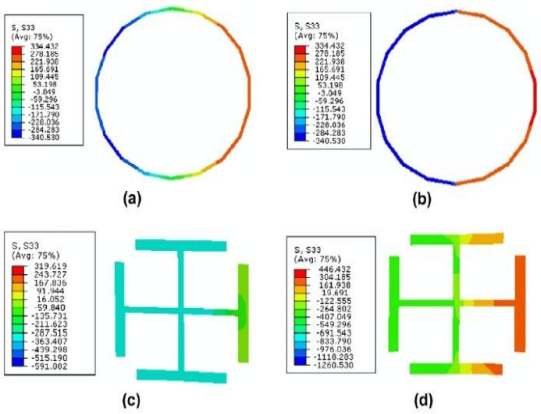

Figure 9. Distribution of longitudinal stresses (a) Cross section of steel pipe at point (1). (b) The cross section of the steel pipe at point (2). (c) The cross section of the steel profile for point (1). (d) The cross section of the steel profile for point (2).[19]

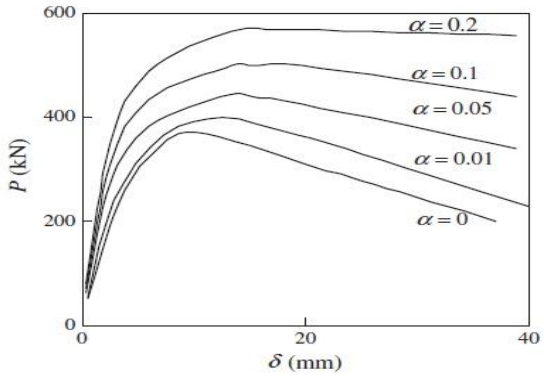

Figure 10. Effect of steel profile ratio on P-δ curve cap for columns[19]

To study the effect of axial loading, 5 different values were selected to formulate the models and the rest of the parameters were assumed to be constant. The computation of p-δ with various levels of axial loading is presented in Fig (11). It can be seen that the curves will continue on line like the previous linear section, although the hardness values are different. In the non-linear section of the curve, an increase in the level of axial loading results in a decrease in the hardness of the section. In the nonlinear phase, the curve decreases with increasing axial load level (n). The axial loading has a downward trend as long as n > 0.3.

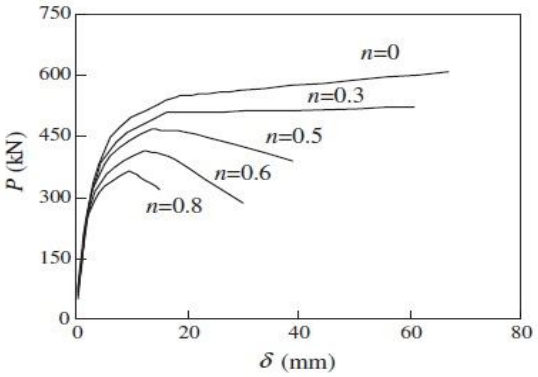

Figure 11. Effect of axial load surface on p-δ cap diagram of SRCFST columns[19]

The effect of the columns loading on the maximum of lateral loading in concrete strength values ranging from 30 to 70 MPa has been indicated in Fig (12). This Fig shows that there is a positive relationship between the concrete strength and the maximum lateral load.

The effect of hollow steel tube thickness on the maximum lateral loading on the member is only examined in the case of hollow circular tubes as they have various thicknesses and other parameters are the same as listed Table (13).

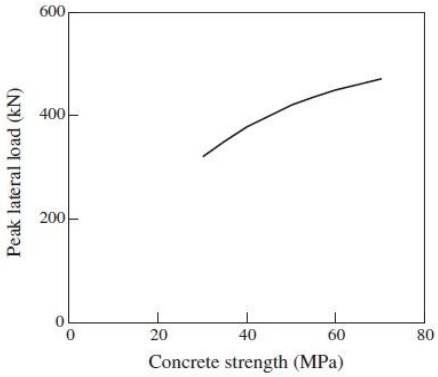

Figure 12. The effect of increasing the strength of concrete on the maximum lateral load[19]

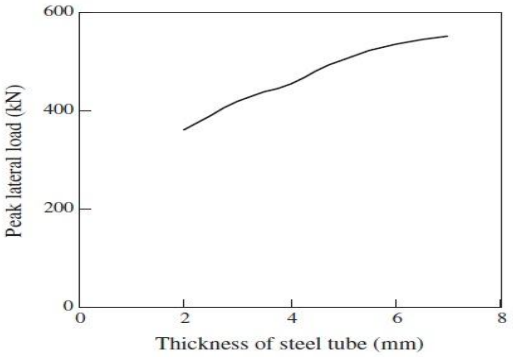

Figure 13. Effect of steel hollow pipe thickness on maximum lateral bearing[19]

Observing the above curve, it can be concluded that the increase in the thickness of steel tube results in an increase in the maximum of lateral load level. All of the specimens with $^{L}/_{B} = 3$ show an almost flexible behavior and they were all tested and controlled on a level surface. Experiment time for all of the square specimens is finished when they are fully ceased. $N - \varepsilon_1$ curves for $S5H10V$ and $S5L10V$ have been presented in Fig (15). Black points represent the local buckling positions in the square steel tube.

The stress-strain curves are normally linear before they reach 80% of their ultimate strength. After this point, the steel starts yielding and the stress-strain curve tends to become curvier. When it reaches the ultimate strength N_u, there will be a decrease in the loading for all of the specimens. The behavior of the specimen after the peak of the curve has an impact on $\rho_{ss}, {}^{B}/_{t}, f_c$, and different failure modes of the specimen. Speciemens of S4hH10,S4H, and their failure modes are discussed as an example in the following. In the case of S4H specimens, which are filled with concrete of high strength $f_c = 70.3Mpa$, when they reach N_y the loading significantly decreases. At this point, two bumps start to appear in the length of the specimens on two opposite sides, and a slip-shear is also observed.Fig (14).

The test is finished when the outer surface of the steel tube in the S4H specimen is fractured and the concrete around it is removed. Fig (14.b) shows that the concrete core is broken along the longtitudal direction of the shear plane. Therefore, it can be deduced that when the diameter-to-thickness ratio is small enough (${}^{B}/_{t} = 43$ in this case), steel tubes are incapable of preventing the slip-shear fractures in high-strength concrete.

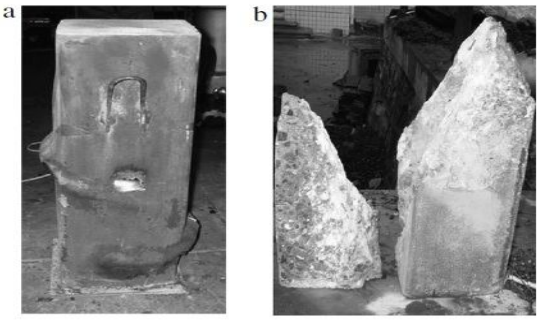

Figure 14. S4H sample failure mode[36]

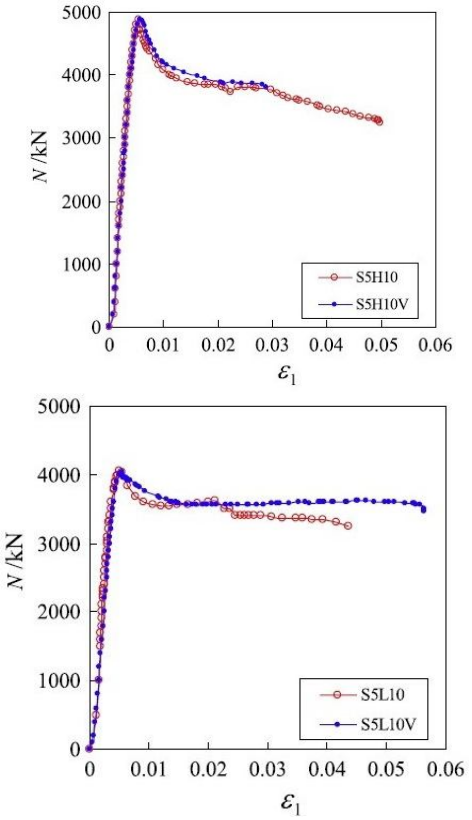

Figure 15. Comparison for samples with or without slipping[36]

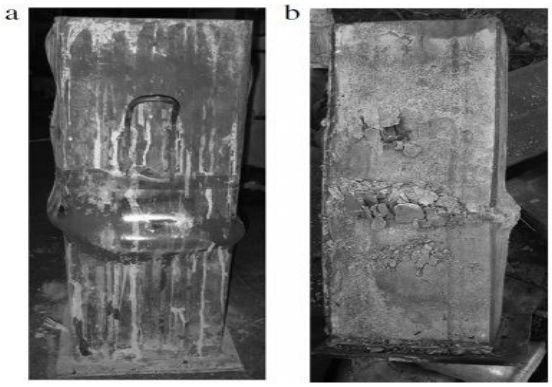

Figure 16. An example of a failure mode in the S4H10 sample[36]

The reduction of strength for S4H10 specimens with steel sections filled with high-strength concrete occurs slowly, and is compared with S4H after the ultimate strength. The buckling of steel tube takes place when the strength remains at a relatively constant value. The testing stoppes when there are several bulges in the length of the specimen.Fig (16). The shear buckling mode can not be clearly observed. Moreover, the greatest amount of bulging occurs in the form of a circle

The stress levels are higher adjacent to the steel tubes resulting in higher confinement of the concrete core. When the steel tubes are removed, it can be observed that concrete is fractured around the bulges but it has maintained its rigidity. Fig (16.b). This analysis demonstrates that the steel section can efficiently prevent the rapid distribution of shear fracture to high-strength concrete. Therefore, this create a change in the type of specimen failure mode.

Loading-axial strain curves have been illustrated in Fig (17). It can be seen from this Fig that the ultimate strength and the maximum of axial strain reduces as the L/B ratio elevates. For L4L10 specimens ($L/B = 9$),L4L10-$L/B = 6$, when the column reaches the ultimate load, the difference in the amount of axial strain among steel cross-sections is within 7%.

Specimens $L4L10 - 12 (L/B = 12)$ reachN_u, the ultimate strength, when the lateral deformation has clearly started expanding. The maximum axial strain is 3.5 larger than the minimum amount, which has been demonstrated by the failure of buckling specimen.

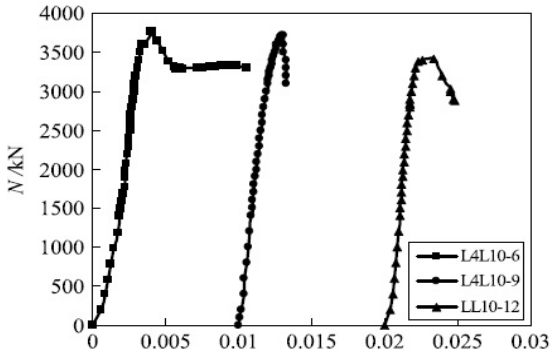

Figure 17. Axial strain curve relative to its load for lean specimens[36]

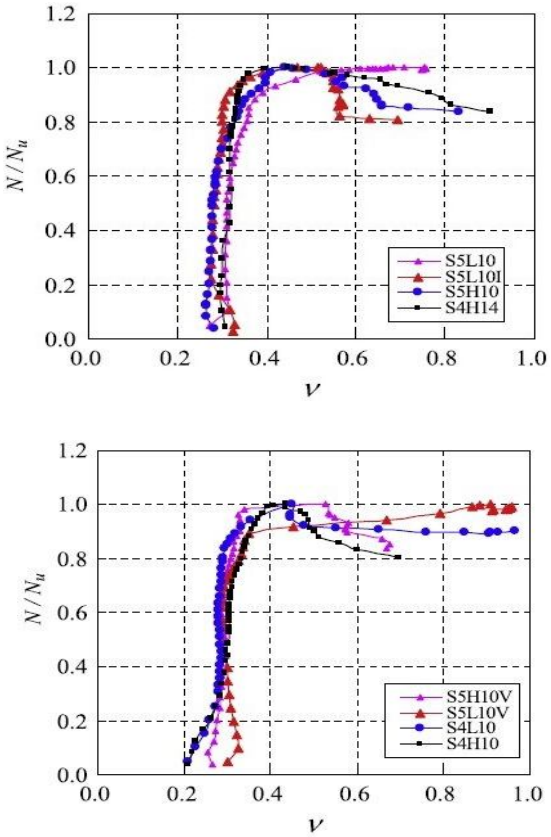

Figure 18. Curve N/N_u of columns[36]

Fig (18) is an indication of a comparison between strain ratio in the steel tube wall and axial load ratio.

The pure strain ratio can be obtained by dividing lateral strain by longitudinal strain. As lateral strain on the sides of square steel tube is variable, therefore the strain values used in Fig (18) are the average amounts of the strain values on two opposite sides in middle of columns obtained by strain gauges. As can be seen in the Fig (18), for axial stress ratio less than 0.8 the strain ratio is almost a constant value which is approximately estimated at poisson's ratio. Strain ratios start increasing in adition to loading level. Varations in strain ratios show that the steel tube creats encloses cocncrete. Steel tube section and the cross-section of steel profile will yield when the specimen is subjected to the ultimate loading.

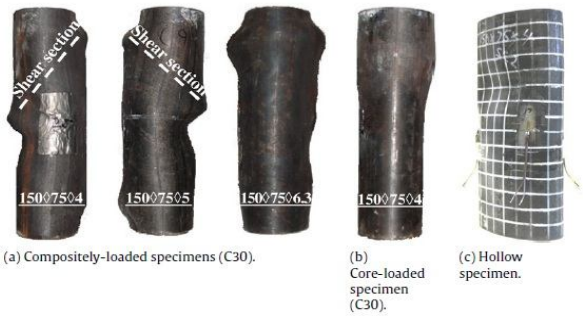

(a) Compositely-loaded specimens (C30). (b) Core-loaded specimen (C30). (c) Hollow specimen.

Figure 19. Modes of failure[17]

4.3. Elliptical composite columns filled with concrete

All of the 21 elliptical specimens filled with concrete were subjected to compression until failure. Different failure modes in compositely-loaded specimens and core-loaded specimens as well as one failure mode for hollow steel tubes without filling concrete have been shown in Fig (19). In case of hollow tubes, both inward and outward buckling is probable as indiacted in Fig (19).

In steel columns filled with concrete inward buckling is prevented by the concrete core in the middle of the column. If local buckling takes place after the deformation of the specimen, it can be observed in Fig (19(a), (b)). Failure modes in specimens subjected to composite loading are similar, exhibiting outward deformation of the elliptical tubes in some cases reveals that various thicknesses result in some differences in the response of the specimens, and a diagonal shear failure in thiner steel tubes (specimens with thicknesses of 4 and 5 mm as illustrated in Fig (19.a)); however, for thicker specimens (with thickness of 6.3 mm) this did not occur. this is believed to be due to the greater confinement offered by the thicker tubes, but owing to the fact that the steel tube was not directly loaded.The short response to the final axial loading of 9 compositely-loaded elliptical specimens (non-greased) has been demonstrated in Figure (20). A summary of the test results as well as some behavioural indices has been provided in Table (8).

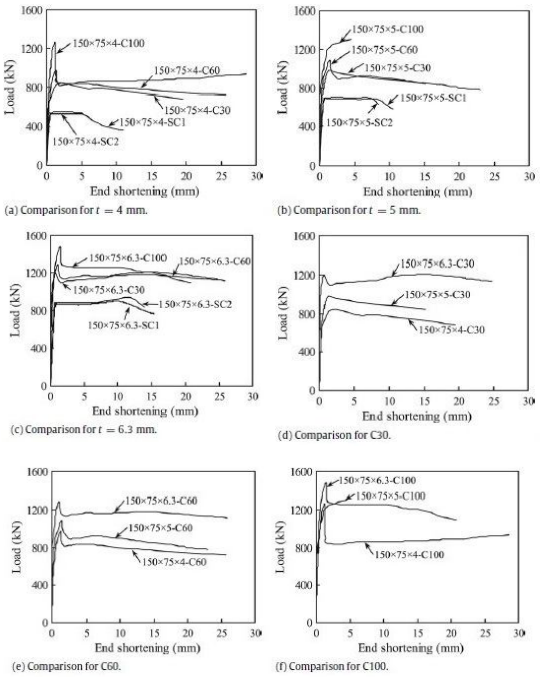

Figure 20. Short end displacement ratio curve to load bearing ratio under different concrete resistances and steel pipe thicknesses[17]

The inner surfaces of 6 specimens were coated with grease to reduce the bond between the concrete and the steel tube, and to simulate the effects of concrete shrinkage. Early research on creep and shrinkage effects in concrete-filled steel tubes generally concluded that creep had a more significant influence on their axial response under static loading.

Table 8. Summary of test results and composite loading behavioral indicators of non-lubricated specimens[17]

Specimen reference	$N_{u,\text{non-greased}}$ (kN)	δ_u (mm)	ξ	CCR	SI	DI
150 × 75 × 4-C30 (NG)	839	1.24	2.44	1.54	1.07	7.4
150 × 75 × 4-C60 (NG)	974	1.35	1.35	1.78	1.01	1.1
150 × 75 × 4-C100 (NG)	1265	1.28	0.73	2.32	0.96	1.0
150 × 75 × 5-C30 (NG)	981	1.45	3.03	1.41	1.12	11.0
150 × 75 × 5-C60 (NG)	1084	1.48	1.65	1.56	1.03	1.5
150 × 75 × 5-C100 (NG)	1296	4.56	0.90	1.86	0.93	–
150 × 75 × 6.3-C30 (NG)	1193	14.67	4.27	1.28	1.12	> 31
150 × 75 × 6.3-C60 (NG)	1280	13.88	2.40	1.38	1.02	> 23
150 × 75 × 6.3-C100 (NG)	1483	7.65	1.26	1.60	0.96	1.9

Table 9. Summary of test results and behavioral indicators of samples under combined loading (lubricated)[17]

Specimen reference	$N_{u,\text{greased}}$ (kN)	δ_u (mm)	ξ	CCR	SI	DI	$N_{u,\text{greased}}/N_{u,\text{non-greased}}$
150 × 75 × 4-C30 (G)	780	1.89	2.46	1.46	1.02	1.75	0.95
150 × 75 × 4-C60 (G)	961	9.90	1.36	1.76	0.99	1.37	0.99
150 × 75 × 4-C100 (G)	1272	1.28	0.74	2.33	0.97	–	1.01
150 × 75 × 5-C30 (G)	988	1.83	3.01	1.42	1.13	> 9.81	1.01
150 × 75 × 5-C60 (G)	1123	1.17	1.67	1.62	1.07	1.54	1.04
150 × 75 × 6.3-C100 (G)	1160	14.38	4.30	1.23	1.06	> 14.6	0.95

However, the common result of both effects is to cause shedding of load from the concrete core to the steel tube. Further experimental studies concluded that although the loss of bond between steel and concrete had relatively little effect on the static behavior of tubes filled with normal strength concrete, marked decreases in resistance caused by loss of bond were observed when high strength concrete was employed_17% for concrete-filled CHS and 14% for concrete-filled.

To investigate shrinkage effects in concrete-filled EHS, 6 greased specimens were tested and the results were compared with those from otherwise similar non-greased specimens. A summary of the test results and behavioural indices for the greased specimens has been listed in Table (9). The results report no more than 5% deviation in ultimate capacity between the $N_{u,greased}$ and $N_{u,non-greased}$ specimens, which is an indication of low effects of shrinkage.

4 - Conclusion:

This paper shows the comparison between numerical and experimental results as well as the accuracy of predicting the behavior of concrete composite columns surrounded by concrete. SRCFST composite columns have higher stiffness and maximum lateral load bearing than CFST columns even with the same geometric parameters and material characteristics. The presence of a steel cross-section also increases the ductility of the column cross-section. Steel cross-sectional wings play a significant role in enclosing the internal concrete of the section. The increase in the strength of structural steel has little effect on the strength of the composite column with a high slimming ratio due to the flexural buckling fracture mode. In general, the strength of SRC composite columns due to the increased yield stress of structural steel for columns with eccentric loading e <0.125 D is noticeable and displayed. In other words, for columns with e> 0.375 D, the effect of the strength of the composite column is effective due to the increase in the yield stress of structural steel for columns with a concrete strength of less than 70 MPa. CFEHS columns are sensitive to the thickness of the steel pipe and its concrete strength. By increasing the thickness of the steel pipe, the result is an increase in the bearing capacity of the sample. It also increases ductility. Increasing the strength of concrete is effective in improving the bearing capacity of the sample. But it reduces the ductility of the sample. The fracture mode is completely different for composite columns with or without steel section. The steel cross-section effectively delays the production of sliding shear cracks in high-strength concretes. L⁄B has a detrimental effect on the final strength of the new columns. Columns with large L⁄B are not recommended for use in engineering practices in

order to take advantage of the moderate effect of confinement between steel pipe and concrete. Square steel pipes can increase the strength and ductility of the concrete core, mainly the insertion of the steel section has an effect on the behavior of the concrete core, and its effect on increasing the strength of the concrete is ignored. For further study, it is also possible to suggest the use of frp sheets in the reinforcement of common composite columns. In this regard, studies on frp sheets have been conducted by Feizbahr et al. [40] and Sadeghian [41, 42], which can be useful.

References

[1] Anslijn, R. and J. Janss, *Le calcul des charges ultimes des colonnes metalliques enrobées de béton*. 1974: Centre de Recherches Scientifiques et Techniques de l'Industrie des Fabrications Métalliques.

[2] Matsui, C., *Study on elasto-plastic behaviour of concrete-encased columns subjected to eccentric axial thrust.* Annual Assembly of Architectural Institute of Japan, 1979: p. 1627-8.

[3] Mirza, S.A. and B. Skrabek, *Statistical analysis of slender composite beam-column strength.* Journal of Structural Engineering, 1992. **118**(5): p. 1312-1332.

[4] Mirza, S.A., V. Hyttinen, and E. Hyttinen, *Physical tests and analyses of composite steel-concrete beam-columns.* Journal of Structural Engineering, 1996. **122**(11): p. 1317-1326.

[5] Chen, C. and S. Yeh. *Ultimate strength of concrete encased steel composite columns*. in *Proceedings of the third national conference on structural engineering*. 1996.

[6] Tsai, K., Y. Lien, and C. Chen, *Behaviour of axially loaded steel reinforced concrete columns.* Journal of the Chinese Institute of Civil and Hydraulic Engineering, 1996. **8**(4): p. 535-545.

[7] Chen, C., et al., *Seismic behaviour and strength of concrete encased steel stub columns and beam–columns.* Report no. MOIS, 1999: p. 881012-1.

[8] El-Tawil, S. and G.G. Deierlein, *Strength and ductility of concrete encased composite columns.* Journal of Structural engineering, 1999. **125**(9): p. 1009-1019.

[9] Dundar, C., et al., *Behaviour of reinforced and concrete-encased composite columns subjected to biaxial bending and axial load.* Building and environment, 2008. **43**(6): p. 1109-1120.

[10] Shanmugam, N.E. and B. Lakshmi, *State of the art report on steel–concrete composite columns.* Journal of constructional steel research, 2001. **57**(10): p. 1041-1080.

[11] Furlong, R.W., *Design of steel-encased concrete beam-columns.* Journal of the Structural Division, 1968. **94**(1): p. 267-281.

[12] Virdi, K., et al., *The ultimate strength of composite columns in biaxial bending.* Proceedings of the institution of civil engineers, 1973. **55**(1): p. 251-272.

[13] Roik ,K. and R. Bergmann, *Design method for composite columns with unsymmetrical cross-sections.* Journal of Constructional Steel Research, 1990. **15**(1-2): p. 153-168.

[14] Kato, B., *Column curves of steel-concrete composite members.* Journal of Constructional Steel Research, 1996. **39**(2): p. 121-135.

[15] Chen, C.-C. and N.-J. Lin, *Analytical model for predicting axial capacity and behavior of concrete encased steel composite stub columns.* Journal of Constructional Steel Research, 2006. **62**(5): p. 424-433.

[16] Elchalakani, M. and X.-L. Zhao, *Concrete-filled cold-formed circular steel tubes subjected to variable amplitude cyclic pure bending.* Engineering Structures, 2008. **30**(2): p. 287-299.

[17] Yang, H., D. Lam, and L. Gardner, *Testing and analysis of concrete-filled elliptical hollow sections.* Engineering Structures, 2008. **30**(12): p. 3771-3781.

[18] Meichun, Z., W. Qingxiang, and F. Xiufen, *Behavior of axially-loaded square steel tube short columns filled with steel-reinforced self-consolidating high-strength concrete* .China Civil Engineering Journal, 2006. **39**(6): p. 35-41.

[19] Chang, X., Y.-Y. Wei, and Y.-C. Yun, *Analysis of steel-reinforced concrete-filled-steel tubular (SRCFST) columns under cyclic loading.* Construction and Building Materials, 2012. **28**(1): p. 88-95.

[20] Shams, M. and M.A. Saadeghvaziri, *State of the art of concrete-filled steel tubular columns.* Structural Journal, 1997. **94**(5): p. 558-571.

[21] Chicoine, T., et al., *Behavior and strength of partially encased composite columns with built-up shapes.* Journal of Structural engineering, 2002. **128**(3): p. 279-288.

[22] Han, L.-H., G.-H. Yao, and X.-L. Zhao, *Tests and calculations for hollow structural steel (HSS) stub columns filled with self-consolidating concrete (SCC).* Journal of Constructional Steel Research, 2005. **61**(9): p. 1241-1269.

[23] Assaad, J., K.H. Khayat, and J. Daczko, *Evaluation of static stability of self-consolidating concrete.* Materials Journal, 2004. **101**(3): p. 207-215.

[24] Chan, T.M. and L. Gardner, *Compressive resistance of hot-rolled elliptical hollow sections.* Engineering structures, 2008. **30**(2): p. 522-532.

[25] Chan, T.M. and L. Gardner, *Bending strength of hot-rolled elliptical hollow sections.* Journal of Constructional Steel Research, 2008. **64**(9): p. 971-986.

[26] Gardner, L., T.M. Chan, and C. Ramos. *Shear resistance of elliptical hollow sections*. in *3rd International Conference on Steel and Composite Structures, ICSCS07-Steel and Composite Structures*. 2007.

[27] Gardner, L. and T.M. Chan, *Cross-section classification of elliptical hollow sections.* Steel and Composite Structures, 2007. **7**(3): p. 185.

[28] Ellobody, E. and B. Young, *Numerical simulation of concrete encased steel composite columns.* Journal of Constructional Steel Research, 2011. **67**(2): p. 211-222.

[29] Sheikh, S.A. and S .Uzumeri, *Analytical model for concrete confinement in tied columns.* Journal of the structural division, 1982. **108**(12): p. 2703-2722.

[30] Mander, J.B., M.J. Priestley, and R. Park, *Theoretical stress-strain model for confined concrete.* Journal of structural engineering, 1988. **114**(8): p. 1804-1826.

[31] Hibbitt, U., *ABAQUS standard user's manual*. Vol. Vol.1.2 and 3 Version 6.8-1. 2008: Karlsson and Sorensen. Inc.

[32] ACI, *Building code requirements for structural concrete and commentary*, A.C. Institute, Editor. 2008, USA.

[33] Richart, F.E., A. Brandtzæg, and R.L. Brown, *A study of the failure of concrete under combined compressive stresses*. 1928, University of Illinois at Urbana Champaign, College of Engineering.

[34] béton, C.e.-i.d., *RC elements under cyclic loading: state of the art report.* 1996.

[35] Guan, P., *Experimental study on ductility of circular steel tubular columns filled with steel-reinforced concrete.* EARTHQUAKE ENGINEERING AND ENGINEERING VIBRATION-CHINESE EDITION, 2003. **23**(1): p. 84-89.

[36] Zhu, M., et al., *Experimental research on square steel tubular columns filled with steel-reinforced self-consolidating high-strength concrete under axial load.* Engineering Structures, 2010. **32**(8): p. 2278-2286.

[37] Dai, X. and D. Lam, *Numerical modelling of the axial compressive behaviour of short concrete-filled elliptical steel columns.* Journal of Constructional Steel Research, 2010. **66**(7): p. 931-942.

[38] Hassanein, M., *Numerical modelling of concrete-filled lean duplex slender stainless steel tubular stub columns.* Journal of constructional steel research, 2010. **66**(8-9): p. 1057-1068.

[39] Ellobody, E., B. Young, and D. Lam, *Behaviour of normal and high strength concrete-filled compact steel tube circular stub columns.* Journal of Constructional Steel Research, 2006. **62**(7): p. 706-715.

[40] Feizbahr, M., et al., *Review on various types and failures of fibre reinforcement polymer.* Middle-East Journal of Scientific Research, 2013. **13**(10): p. 1312-1318.

[41] Sadeghian, S., *Retrofit of the Concrete Structures by CFRP Sheets against Explosion.* Journal of Civil Engineering Researchers, 2020. **3**(1): p. 1-5.

[42] Sadeghian, S., *Investigation of thickness and number of layers of CFRP sheets in reinforcement of concrete slab under blast load*. 2015, Zenodo.